Spontaneous Symmetry Breaking of an Optical Polarization State in a Polarization-Selective Nonlinear Resonator

K. S. Manannikov[1,*], E. I. Mironova[1], A. S. Poliakov[1], A. Mikhaylov[2], A. E. Ulanov[3], and A. I. Lvovsky[4]

[1] Department of Physics of Complex Systems, Weizmann Institute of Science, Israel
[2] Q.ANT GmbH, Handwerkstr. 29, 70565 Stuttgart, Germany
[3] Deutsches Elektronen-Synchrotron DESY, Notkestr. 85, 22607 Hamburg, Germany
[4] Clarendon Laboratory, University of Oxford, Oxford OX1 3PU, UK
[*] konstantin.manannikov@weizmann.ac.il

Compiled November 22, 2024

We exploit polarization self-rotation in atomic rubidium vapor to observe spontaneous symmetry breaking and bistability of polarization patterns. We pump the vapor cell with horizontally polarized light while the vertical polarization, which is initially in the vacuum state, is resonated in a ring cavity. Microscopic field fluctuations in this mode experience cumulative gain due to the compound action of amplification due to the self-rotation and feedback through the resonator, eventually acquiring a macroscopic magnitude akin to an optical parametric oscillator. The randomness of these fluctuations results in a bistable, random macroscopic polarization pattern at the output. We propose utilizing this mechanism to simulate Ising-like interaction between multiple spatial modes and as a basis for a fully optical coherent Ising machine.

http://dx.doi.org/10.1364/ao.XX.XXXXXX

A nonlinear optical effect known as polarization self-rotation (PSR) occurs as a result of the interaction of an elliptically polarized light with a nonlinear $\chi^{(3)}$ medium. PSR consists in the rotation of the polarization ellipse at a rate that increases with the ellipticity [Fig. 1(a)]. In a Kerr medium, the refractive index for each component depends on its intensity. Unequal refractive indices result in different phase velocities, which in turn leads to a rotation of the polarization ellipse [Fig. 1(b)].

Initially investigated in the 1970s [1], PSR gained renewed attention in the early 2000s, when it was considered as a simple source of squeezed light [2–4]. When a PSR-exhibiting medium is pumped with linearly (e.g., horizontally) polarized light, microscopic field fluctuations in the orthogonal (vertical) polarization mode can manifest as microscopic ellipticity of the overall polarization pattern. Microscopic self-rotation due to this ellipticity brings about linear shear of the phase space of the vertical polarization mode, squeezing the uncertainty circle.

In this work, we experimentally investigate the optical parametric oscillation (OPO) induced by PSR. To that end, the effect on the vertical mode is enhanced by a cavity in which that mode resonates [Fig. 1(c)]. For certain resonator lengths, the amplification becomes cumulative, leading to a macroscopic electromagnetic field amplitude in the steady state and thus to a macroscopic ellipticity of the field polarization in the vapor cell.

Our PSR-based OPO shows a spontaneous symmetry breaking of the optical polarization state. The handedness of the elliptical pattern in the steady-state is determined by the sign of the initial fluctuation from which it originated. Consequently, this handedness is random every time the parametric oscillation is initiated and remains constant for as long as the oscillation is sustained. In other words, the polarization state is bistable.

Bistability is a common feature of parametric oscillators and Kerr cavities, observed in a variety of schemes [5–8]. For example, Moroney *et al.* [9] observed polarization bistability with a continuous wave in a high-Q fiber resonator with Kerr nonlinearity. Due to spontaneous symmetry breaking, one circular component of the linearly polarized input light became dominant inside the cavity, while the other one was reflected.

Bistable systems can be affected by various asymmetries introducing a bias in the final binary distribution [9–12]. In our scheme, the main source of the signal's polarization bias is the leakage of the pump in the cavity feedback loop. However, polarization selectivity of the resonator in combination with the full control of the pump polarization allow us to minimize that leak and observe random selection of one of the two helicities in the output.

Atomic resonant enhancement in our system leads to a much stronger nonlinearity than the $\chi^{(3)}$ nonlinearity in a fiber or the $\chi^{(2)}$ nonlinearity in a crystal: significant squeezing of a continuous wave mode can be obtained in a single pass through the vapor cell. This makes the scheme attractive for the implementation of an all-optical coherent Ising machine. We discuss this idea at the end of the paper.

We analyze the transformation of the field polarization pattern under the joint action of PSR and the resonator. Interacting with a rubidium vapor cell, elliptically polarized light experi-

ences rotation of its optical axis by the angle $\varphi(\varepsilon)$, where ε is the ellipticity. Subsequently, the vertical polarization is reflected by a polarizing beam splitter into the resonator [Fig. 1(c)]. During a roundtrip through the resonator, the field accrues a phase shift ψ and experiences a linear loss before being re-injected into rubidium. The field transformation in one roundtrip can thus be written as follows:

$$\begin{pmatrix} \mathcal{E}_H \\ \mathcal{E}_V^{(n+1)} \end{pmatrix} = \begin{pmatrix} 0 & 0 \\ 0 & \sqrt{\eta}e^{i\psi} \end{pmatrix} \begin{pmatrix} \cos(\varphi) & -\sin(\varphi) \\ \sin(\varphi) & \cos(\varphi) \end{pmatrix} \begin{pmatrix} \mathcal{E}_H \\ \mathcal{E}_V^{(n)} \end{pmatrix} + \begin{pmatrix} \mathcal{E}_H \\ 0 \end{pmatrix}, \quad (1)$$

where $\mathcal{E}_H$, $\mathcal{E}_V$ are the complex field amplitudes of the polarization components in the nth roundtrip and $1-\eta$ is the intensity loss in the cavity per roundtrip.

Fig. 1(d) visualizes the evolution of $\mathcal{E}_V$ in the complex plane. We use the horizontal component as phase reference, so $\mathcal{E}_H$ is a real number. PSR admixes this real horizontal amplitude into the vertical mode [Fig. 1(d,ii)]. The subsequent roundtrip through the resonator rotates the complex phase of the field and scales it by factor $\sqrt{\eta}$ [Fig. 1(d,iii)]. The resulting vector undergoes further horizontal displacement due to self-rotation (determined by the new ellipticity) [Fig. 1(d,iv)], and so on.

To identify the conditions under which this recurrent transformation leads to oscillation, we assume the initial ellipticity to be small ($\varepsilon \ll 1$). The self-rotation angle is then proportional to the ellipticity [2]:

$$\varphi \approx gl\varepsilon, \quad (2)$$

where the proportionality coefficient g depends on the intensity of the incident light and its detuning from resonance. The ellipticity itself (for $\mathcal{E}_H \in \mathbb{R}$) is defined as $\epsilon = \arcsin \frac{\mathcal{E}_H \mathrm{Im}\mathcal{E}_V}{|\mathcal{E}_H|^2 + |\mathcal{E}_V|^2}$ [2], simplifying to $\varepsilon \approx \frac{\mathrm{Im}\mathcal{E}_V}{\mathcal{E}_H}$ for $\varepsilon \ll 1$. The vertical field component transformation according to Eq. (1) then becomes

$$\mathcal{E}_V^{(n+1)} \approx \sqrt{\eta}e^{i\psi}(\mathcal{E}_V + gl\mathrm{Im}\mathcal{E}_V). \quad (3)$$

The threshold condition corresponds to $\left|\mathcal{E}_V^{(n+1)}\right| > \left|\mathcal{E}_V^{(n)}\right|$. This inequality can be solved by writing Eq. (3) in the matrix form with respect to the real and imaginary parts of $\mathcal{E}_V$ and finding the eigenvalues $\lambda_{1,2}$ of the transfer matrix. The threshold condition is obtained by requiring $\max_\psi(|\lambda_{1,2}|) > 1$, which resolves to

$$gl > 1/\sqrt{\eta} - \sqrt{\eta}, \quad (4)$$

with the highest gain observed at

$$\psi = \arctan\left(\frac{gl}{2}\right). \quad (5)$$

The infinite growth of $|\mathcal{E}_V|$ is limited by the pump depletion and saturation of the self-rotation coefficient for large ellipticities.

To obtain the polarization of the field in the steady state, the small-ellipticity condition must be relaxed, and Eq. (1) must be solved numerically.

The bistability of this PSR-based OPO can be understood by examining the top and bottom rows of Fig. 1(d). As is evident from Eq. (3), the sign of the imaginary component of $\mathcal{E}_V$ (and hence the helicity of the polarization pattern) is preserved in each roundtrip through the resonator. Depending on the initial value

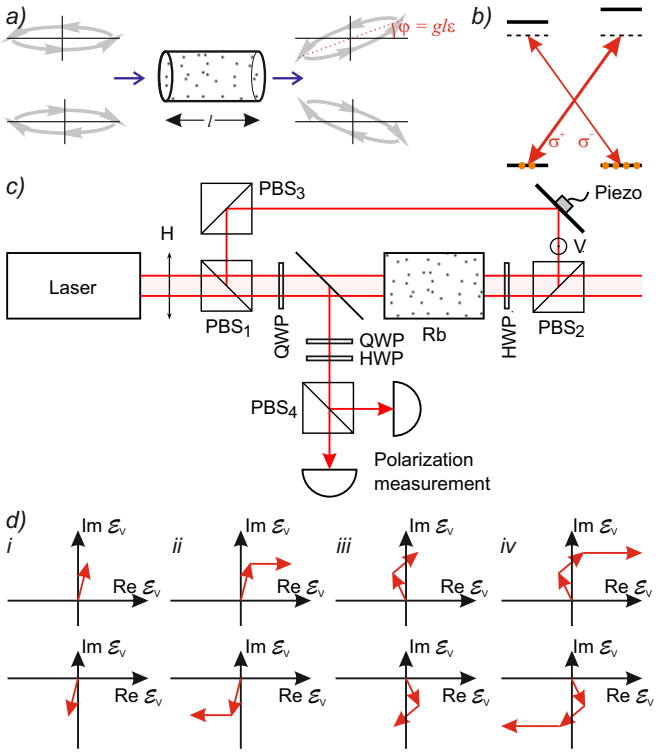

Fig. 1. Concept of the study. a) PSR effect. The magnitude and direction of self-rotation depend on the ellipticity of the input polarization and its handedness, respectively. b) Conceptual explanation in an atomic X-system. Elliptically polarized light is described as a sum of two circular components (σ_+ and σ_-) with unequal intensities, interacting with the respective transitions in the X-system. These components experience different refractive indices due to optical pumping and ac Stark shift. c) Scheme of the experiment. Rubidium vapor is pumped by horizontally polarized light, while the vertical polarization is resonated in a ring cavity. PBS: polarizing beam splitter; HWP: half-wave plate; QWP: quarter-wave plate. d) Origin of optical parametric oscillation and bistability. Complex electric field vector of the vertical polarization component is shown: (i) before entering the vapor cell, (ii) after passing through the cell and experiencing PSR, (iii) after a roundtrip through the cavity, before entering the cell for the second time, (iv) after second passage through the cell. The phase of the developed oscillation depends on the sign of the initial $\mathrm{Im}\mathcal{E}_V$, giving rise to bistability (see text for further details).

of this sign, $\mathcal{E}_V$ will acquire one of the two opposite phases when amplified. Because the self-rotation angle $\varphi(\varepsilon)$ is an odd function of the ellipticity, it follows that whenever a vector $(\mathcal{E}_H, \mathcal{E}_V)$ with ellipticity ε is a steady state solution of Eq. (1), so is the vector $(\mathcal{E}_H, \mathcal{E}_V^*)$ with ellipticity $-\varepsilon$.

For the experiment, we utilize a Vitawave external-cavity diode laser, which emits continuous-wave light at 795 nm with a power of 13.5 mW, resonant with the D_1 transition in ^{85}Rb. For PSR measurements, the laser is set to horizontal polarization and directed into a rubidium cell heated to 70°C and placed inside a telescope formed by two $f = 30$ cm lenses. The transmitted beam is subjected to polarimetric balanced detection in a 45° basis (see Supplementary 1 for more experimental details).

The self-rotation is measured as a function of the laser detun-

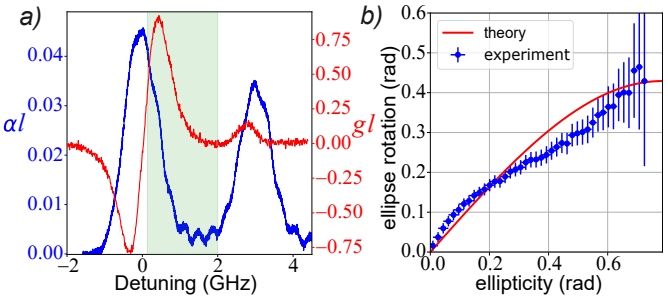

Fig. 2. Experimental observation of PSR. Data for both plots are acquired at the pump power $P = 13.5$ mW. a) Coefficient of absorption αl (blue line, left scale) and self-rotation parameter gl (red line, right scale) measured across the ^{85}Rb D1 transition. Zero detuning corresponds to the maximum absorption wavelength. The absorption coefficient αl is calculated as the natural logarithm of the ratio of the transmitted and input intensities. The green region marks the frequency range where bistability is observed. b) Dependence of the polarization ellipse rotation angle on initial ellipticity at frequency detuning $\Delta = 0.35$ GHz. Experimental data (blue dots) is compared to the theoretically obtained curve (red line) from Eq. (6).

ing [Fig. 2(a)] and ellipticity [Fig. 2(b)]. For the latter dependence, we also obtain a theoretical prediction based on an X-shaped level structure [Fig. 1(b)] (more details in Supplementary 2):

$$\varphi = \frac{C\delta \sin(2\varepsilon)}{(2+8\delta^2) + [1+\cos(4\varepsilon)]I/I_{\text{sat}}}, \tag{6}$$

where I is the optical intensity, I_{sat} the saturation intensity of the transition, δ the ratio of the detuning and the resonance line width, and C a proportionality coefficient. A good fit to the experimental data is found for $\delta = 0.1$ and $I/I_{\text{sat}} = 10$. We can see that the proportionality $\varphi \propto \varepsilon$ holds for small ellipticities. The difference between the experimental and theoretical curves is due to simplified treatment of the complex rubidium energy structure as a four-level system without Doppler broadening.

To observe bistability, we build the setup shown in Fig. 1(c) (see Supplementary 4 for details). The laser is tuned into the range with the lowest losses and the highest nonlinearity [shown in pale green in Fig. 2(a)]. A small fraction of the field is deflected from the cavity before the cell with a highly transmissive beam splitter, which was tested to have a negligible effect on the relative phase of the horizontal and vertical polarization. The reflected beam is subjected to polarimetric measurement in the circular basis via two photodetectors. The pump polarization is carefully adjusted by two waveplates to eliminate leakage into the cavity in the absence of PSR.

The signal from these photodetectors, while the phase of the resonator is scanned with a piezoelectric transducer, is shown in Fig. 3(a). Whenever the phase passes through a cavity resonance, oscillation emerges with randomly either the right or left circular component being prevalent.

To investigate the dependence of the bistable state on the losses in the resonator, we measure the output polarization in circular and canonical bases to evaluate (see Supplementary 3 for a derivation):

$$\frac{\text{Im}\mathcal{E}_V}{\mathcal{E}_H} = \frac{I_L - I_R}{2I_H} \text{ and } \frac{\text{Re}\mathcal{E}_V}{\mathcal{E}_H} = \frac{\sqrt{I_V - (\text{Im}\mathcal{E}_V)^2}}{\mathcal{E}_H}, \tag{7}$$

where I_R, I_L, and I_H are the intensities of the right circular, left circular, and horizontal polarization components respectively.

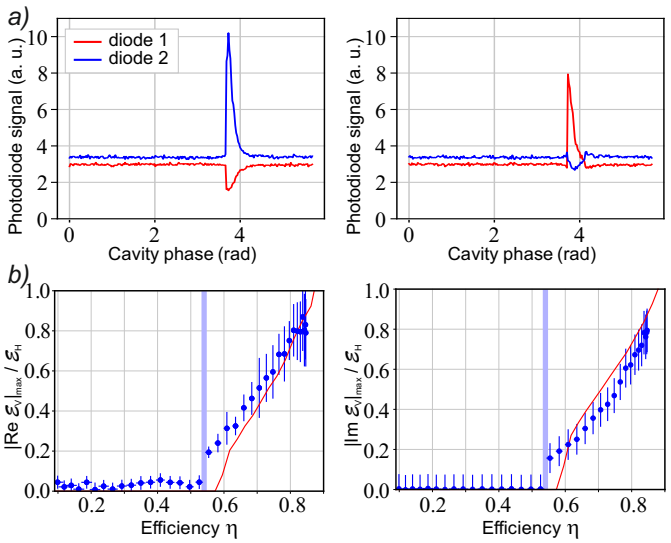

Fig. 3. Bistability measurements. a) Signals from the two photodiodes performing polarization measurements in the circular basis during two successive phase scans of the cavity. b) Real and imaginary parts of the steady-state vertical amplitude as a function of loss in the resonator. The red theoretical curve is obtained by numerically solving Eq. (1) with the self-rotation angle computed from Eq. (6). The blue shaded area shows the threshold calculated from Eq. (4) with the self-rotation parameter g obtained from the data in Fig. 2(b). All measurements are performed with a fixed frequency detuning $\Delta = 0.35$ GHz and pump power $P = 13.5$ mW. Small non-zero values of $\text{Re}\mathcal{E}_V$ under the threshold is due to imperfect balancing of the polarization measurement.

The resulting data are demonstrated in Fig. 3(b). We observe that the bistability is significantly tolerant to losses, a consequence of a high phase-dependent gain in each roundtrip.

To demonstrate the randomness of the bistable states, we acquire a series of $M = 700$ oscillation events, ascribe a value $s_n = \pm 1$ to each event according to its helicity, and calculate the auto-correlation

$$K(m) = \frac{1}{M}\sum_{n=0}^{M} s_n \cdot s_{n+m}. \tag{8}$$

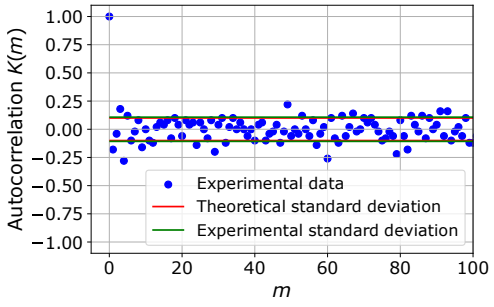

Fig. 4. Auto-correlation function for experimental values of binary phases (blue dots). Double standard deviation intervals for the experimental auto-correlation function and for the auto-correlation function of the ideal independent binary distribution are also shown.

As can be seen in Fig. 4, this function behaves similarly to that of a fair coin: the standard deviations of $K(m)$ (for $m \neq 0$) for the experimental data and ideal Bernoulli distributions are almost equal. This suggests that the randomness observed is likely to originate from quantum vacuum fluctuations, as is normally the case with OPOs [10]. However, it cannot be excluded that the fluctuations are of classical origin, such as fast oscillations of the pump polarization or external magnetic field.

Such randomness can be a basis for a random number generator [10, 11]. While the random data in this experiment are acquired at a rate limited by the cavity scan speed, a more fundamental physical limitation is imposed by the atomic relaxation time and the duration of several roundtrips through the resonator, both on time scales of tens of nanoseconds. Higher rates can be obtained by spatial demultiplexing, as discussed below.

In summary, we demonstrated that polarization self-rotation could be utilized to generate bistable polarization states of light. Spontaneous symmetry breaking for the initially horizontally polarized light was achieved thanks to the resonant optical nonlinearity of rubidium vapor cell in a vertical polarization selective resonator. As a result, the field in the resonator becomes elliptically polarized with a random helicity, as evidenced by statistical analysis.

The optical system presented in this paper can be scaled up: several independent bistable spatial modes can be obtained simultaneously by focusing multiple spatially separated laser beams in the same vapor cell. These modes can be arbitrarily coupled by placing a spatial light modulator into the resonator using spatial matrix-vector multiplication methods developed in the context of optical neural networks [13, 14]. This system of coupled optical parametric oscillators would implement an all-optical coherent Ising machine (CIM), i.e. an analog optical neural network capable of evolving into the ground state of an Ising Hamiltonian [15, 16].

In the original optoelectronic CIM [17–19], the pulsed modes are coupled through classical measurement and feedback, which precludes their entanglement and hence quantum computational advantage [20]. An all-optical CIM, in which the interaction between modes occurs via interference, would address this shortcoming. Existing solutions, based on pulsed modes and fiber interferometers, either involved very few oscillators [21] or had the coupling limited to nearest neighbors [22]. Leveraging the resolution of spatial light modulators to couple spatially separated continuous-wave bistable modes appears to be a promising path toward scalability. The number of modes in this setting is then limited by the vapor cell area. While each mode in the cell is $\lesssim 0.25$ mm wide, spurious cross-talk between modes may impose a lower limit on the distance between neighboring modes. This effect can be curtailed by constructing an array of microcells with longitudinal partitioning.

In addition to applications for combinatorial optimization, it is interesting to explore the potential of this all-optical CIM as a quantum simulator of condensed matter physics. Such studies have been actively pursued with the D-Wave annealer, such as e.g. a recent simulation of nonequilibrium dynamics of a magnetic spin system undergoing a quantum phase transition [23]. The promise of multiple coupled OPOs in this context has been shown theoretically [24, 25], but experimental research has so far been limited to the optoelectronic scheme [26].

The bistability, especially near the exceptional point, is highly sensitive to fluctuations of the system parameters, particularly an external magnetic field. Hence the setup may also prove promising as a magnetic field sensor.

We believe the system presented in this work offers significant potential for many academic and practical applications in quantum optics and analog computing.

Funding. AL's research is supported by the Innovate UK Smart Grant 10043476 and the EPSRC Grant EP/Y020596/1.

Acknowledgment. We are grateful to A. V. Masalov for support in the experiment and fruitful discussions.

Disclosures. The authors declare no conflicts of interest.

Data Availability Statement. The data presented here are available from the corresponding author upon request.

Supplemental document. See Supplement for supporting content.

REFERENCES

1. P. Maker, R. Terhune, and C. Savage, Phys. Rev. Lett. **12**, 507 (1964).
2. A. Matsko, I. Novikova, G. R. Welch, *et al.*, Phys. Rev. A **66**, 043815 (2002).
3. J. Ries, B. Brezger, and A. Lvovsky, Phys. Rev. A **68**, 025801 (2003).
4. E. E. Mikhailov and I. Novikova, Opt. letters **33**, 1213 (2008).
5. N. I. Zheludev, Sov. Phys. Uspekhi **32**, 357 (1989).
6. D. J. Gauthier, M. S. Malcuit, and R. W. Boyd, Phys. Rev. Lett. **64**, 1721 (1990).
7. D. J. Gauthier, M. S. Malcuit, A. L. Gaeta, and R. W. Boyd, Phys. Rev. Lett. **64**, 1721 (1990).
8. S. Coen, B. Garbin, G. Xu, *et al.*, Nat. Comms. **15**, 1398 (2024).
9. N. Moroney, L. Del Bino, S. Zhang, *et al.*, Nat. Comms. **13**, 398 (2022).
10. T. Steinle, J. N. Greiner, J. Wrachtrup, *et al.*, Phys. Rev. X **7**, 041050 (2017).
11. L. Quinn, G. Xu, Y. Xu, *et al.*, Opt. Lett. **48**, 3741 (2023).
12. B. Garbin, J. Fatome, G.-L. Oppo, *et al.*, Phys. Rev. Res. **2**, 023244 (2020).
13. J. Spall, X. Guo, and A. I. Lvovsky, Optica **9**, 803 (2022).
14. L. Bernstein, A. Sludds, C. Panuski, *et al.*, Sci. Adv. **9**, eadg7904 (2023).
15. M. Calvanese Strinati, I. Aharonovich, S. Ben-Ami, *et al.*, New J. Phys. **22**, 085005 (2020).
16. M. Calvanese Strinati, L. Bello, E. G. Dalla Torre, and A. Pe'er, Phys. Rev. Lett. **126**, 143901 (2021).
17. T. Inagaki, Y. Haribara, K. Igarashi, *et al.*, Science **354**, 603 (2016).
18. P. L. McMahon, A. Marandi, Y. Haribara, *et al.*, Science **354**, 614 (2016).
19. T. Honjo, T. Sonobe, K. Inaba, *et al.*, Sci. Adv. **7**, eabh0952 (2021).
20. E. S. Tiunov, A. E. Ulanov, and A. I. Lvovsky, Opt. Express **27**, 10288 (2019).
21. A. Marandi, Z. Wang, K. Takata, *et al.*, Nat. Photon. **8**, 937 (2014).
22. T. Inagaki, K. Inaba, R. Hamerly, *et al.*, Nat. Photon. **10**, 415 (2016).
23. A. D. King, A. Nocera, M. M. Rams, *et al.*, arXiv preprint arXiv:2403.00910 (2024).
24. M. Calvanese Strinati, L. Bello, A. Pe'er, and E. G. Dalla Torre, Phys. Rev. A **100**, 023835 (2019).
25. L. Bello, M. Calvanese Strinati, E. G. Dalla Torre, and A. Pe'er, Phys. Rev. Lett. **123**, 083901 (2019).
26. H. Takesue, Y. Yamada, K. Inaba, *et al.*, Phys. Rev. Appl. **19**, L031001 (2023).

FULL REFERENCES

1. P. Maker, R. Terhune, and C. Savage, "Intensity-dependent changes in the refractive index of liquids," Phys. Rev. Lett. **12**, 507 (1964).
2. A. Matsko, I. Novikova, G. R. Welch, *et al.*, "Vacuum squeezing in atomic media via self-rotation," Phys. Rev. A **66**, 043815 (2002).
3. J. Ries, B. Brezger, and A. Lvovsky, "Experimental vacuum squeezing in rubidium vapor via self-rotation," Phys. Rev. A **68**, 025801 (2003).
4. E. E. Mikhailov and I. Novikova, "Low-frequency vacuum squeezing via polarization self-rotation in rb vapor," Opt. letters **33**, 1213–1215 (2008).
5. N. I. Zheludev, "Polarization instability and multistability in nonlinear optics," Sov. Phys. Uspekhi **32**, 357 (1989).
6. D. J. Gauthier, M. S. Malcuit, and R. W. Boyd, "Polarization instabilities of counterpropagating laser beams in sodium vapor," Phys. Rev. Lett. **64**, 1721 (1990).
7. D. J. Gauthier, M. S. Malcuit, A. L. Gaeta, and R. W. Boyd, "Polarization bistability of counterpropagating laser beams," Phys. Rev. Lett. **64**, 1721 (1990).
8. S. Coen, B. Garbin, G. Xu, *et al.*, "Nonlinear topological symmetry protection in a dissipative system," Nat. Comms. **15**, 1398 (2024).
9. N. Moroney, L. Del Bino, S. Zhang, *et al.*, "A kerr polarization controller," Nat. Comms. **13**, 398 (2022).
10. T. Steinle, J. N. Greiner, J. Wrachtrup, *et al.*, "Unbiased all-optical random-number generator," Phys. Rev. X **7**, 041050 (2017).
11. L. Quinn, G. Xu, Y. Xu, *et al.*, "Random number generation using spontaneous symmetry breaking in a kerr resonator," Opt. Lett. **48**, 3741–3744 (2023).
12. B. Garbin, J. Fatome, G.-L. Oppo, *et al.*, "Asymmetric balance in symmetry breaking," Phys. Rev. Res. **2**, 023244 (2020).
13. J. Spall, X. Guo, and A. I. Lvovsky, "Hybrid training of optical neural networks," Optica **9**, 803–811 (2022).
14. L. Bernstein, A. Sludds, C. Panuski, *et al.*, "Single-shot optical neural network," Sci. Adv. **9**, eadg7904 (2023).
15. M. Calvanese Strinati, I. Aharonovich, S. Ben-Ami, *et al.*, "Coherent dynamics in frustrated coupled parametric oscillators," New J. Phys. **22**, 085005 (2020).
16. M. Calvanese Strinati, L. Bello, E. G. Dalla Torre, and A. Pe'er, "Can nonlinear parametric oscillators solve random ising models?" Phys. Rev. Lett. **126**, 143901 (2021).
17. T. Inagaki, Y. Haribara, K. Igarashi, *et al.*, "A coherent ising machine for 2000-node optimization problems," Science **354**, 603–606 (2016).
18. P. L. McMahon, A. Marandi, Y. Haribara, *et al.*, "A fully programmable 100-spin coherent Ising machine with all-to-all connections," Science **354**, 614–617 (2016).
19. T. Honjo, T. Sonobe, K. Inaba, *et al.*, "100,000-spin coherent ising machine," Sci. Adv. **7**, eabh0952 (2021).
20. E. S. Tiunov, A. E. Ulanov, and A. I. Lvovsky, "Annealing by simulating the coherent Ising machine," Opt. Express **27**, 10288–10295 (2019).
21. A. Marandi, Z. Wang, K. Takata, *et al.*, "Network of time-multiplexed optical parametric oscillators as a coherent Ising machine," Nat. Photon. **8**, 937 (2014).
22. T. Inagaki, K. Inaba, R. Hamerly, *et al.*, "Large-scale Ising spin network based on degenerate optical parametric oscillators," Nat. Photon. **10**, 415–419 (2016).
23. A. D. King, A. Nocera, M. M. Rams, *et al.*, "Computational supremacy in quantum simulation," arXiv preprint arXiv:2403.00910 (2024).
24. M. Calvanese Strinati, L. Bello, A. Pe'er, and E. G. Dalla Torre, "Theory of coupled parametric oscillators beyond coupled ising spins," Phys. Rev. A **100**, 023835 (2019).
25. L. Bello, M. Calvanese Strinati, E. G. Dalla Torre, and A. Pe'er, "Persistent coherent beating in coupled parametric oscillators," Phys. Rev. Lett. **123**, 083901 (2019).
26. H. Takesue, Y. Yamada, K. Inaba, *et al.*, "Observing a phase transition in a coherent ising machine," Phys. Rev. Appl. **19**, L031001 (2023).